EUROPEAN ORGANIZATION FOR NUCLEAR RESEARCH

CERN-EP/84-161
29 November 1984

NUCLEAR SPINS, MOMENTS, AND CHANGES OF THE MEAN SQUARE CHARGE RADII OF $^{140-153}$Eu

S.A. Ahmad[1] and W. Klempt
CERN, Geneva, Switzerland

C. Ekström
Chalmers University of Technology, Gothenburg, Sweden

R. Neugart and K. Wendt[2]
Institut für Physik, Universität Mainz, Mainz,
Fed. Rep. Germany

ISOLDE Collaboration, CERN, Geneva, Switzerland

ABSTRACT

The hyperfine structures and isotope shifts of 14 isotopes of Eu (Z = 63) in the mass range $140 \leq A \leq 153$, partly with isomeric states, have been measured in the atomic transitions at 4594 Å and 4627 Å, using the technique of collinear fast-beam laser spectroscopy at the ISOLDE facility at CERN. The nuclear spins, the magnetic dipole and electric quadrupole moments, and the changes in the mean square charge radii have been evaluated. These nuclear parameters clearly reflect the effects of the N = 82 neutron-shell closure in the single-proton hole states with respect to the semi-magic gadolinium (Z = 64), and the N = 88-90 shape transition.

(Submitted to Zeitschrift für Physik A)

---

1) On leave from Bhabha Atomic Research Centre, Bombay, India.
2) Present address: CERN, Geneva, Switzerland.

1. INTRODUCTION

The spins, electromagnetic moments, and mean square charge radii of the nuclear ground and isomeric states serve as a valuable aid in understanding the single-particle and collective aspects of nuclear structure, especially in the regions of shell closure or shape transition. Both these phenomena occur in the rare-earth region at the neutron numbers N = 82 and N = 88-90. At present, the nuclides around these neutron numbers are accessible to laser-spectroscopic measurements of the hyperfine structure (hfs) and the isotope shift (IS) for almost all elements between barium (Z = 56) and ytterbium (Z = 70) [1]. A systematic investigation is in progress for the isotopic chains of the even-Z elements, including the neutron-rich Ba isotopes [2] and the neutron-deficient Gd, Dy, Er, and Yb isotopes [1,3]. The aim of these studies is to have a rather complete mapping of the single-particle properties and deformations as one goes from spherical shapes (N = 82) to strongly deformed ones (N $\geq$ 90). The behaviour of the N = 88-90 isotopes is of particular interest. In the elements close to gadolinium (Z = 64) they exhibit a pronounced shape transition which diminishes in the lighter as well as in the heavier elements and is probably related to the Z = 64 proton-subshell closure.

Europium (Z = 63), with a single-proton hole in the $2d_{5/2}$ subshell, should be the prominent odd-Z candidate for demonstrating the influence of the unpaired proton on the development of deformation and the neighbourhood of the closed subshell on the single-particle states. From an atomic-physics point of view, Eu has a relatively simple electronic structure due to the half-filled 4f shell. The two stable isotopes, ^{151}Eu and ^{153}Eu, have for a long time been the outstanding example of a nuclear shape transition discovered in the spectroscopic quadrupole moments and later found to manifest themselves also in the exceptionally large isotope shift, even in comparison with the neighbouring even-Z elements [4].

Recently there has been a considerable interest in measuring the magnetic moments and isotope shifts of the radioactive isotopes of Eu. The magnetic dipole moments μ of the isotopes $^{145-149}$Eu have been determined, using the nuclear-orientation technique (NO), by van den Berg et al. [5] and Kracikova et al. [6] with contradictory results. In parallel to the present work, Alkhazov et al. [7]

have measured the IS in the 5765 Å line of Eu I for $^{141-150}$Eu, using the technique of laser multistep photoionization and, very recently, Dörschel et al. [8] have published IS and hfs data for ^{147}Eu, ^{149}Eu, and $^{151-156}$Eu, obtained by collinear ion beam-laser spectroscopy in the 6049 Å line of Eu II. These latter data, mainly on the neutron-rich isotopes, are complementary to our results. The spins I of ^{143}Eu, $^{145-150}$Eu, and ^{156}Eu had been measured earlier by Ekström et al. [9,10], using the technique of atomic beam magnetic resonance (ABMR).

Precise electric quadrupole moments Q_s of the two stable isotopes, ^{151}Eu and ^{153}Eu, have been reported recently by Tanaka et al. [11] from measurements of the quadrupole hyperfine splitting energies of the muonic M X-rays. Prior to this study, the reference values of Q_s were known only from the analyses of optical hfs [12] involving considerable uncertainties of the electric field gradient at the nucleus.

We have investigated the hfs and IS in the isotopic chain of $^{140-153}$Eu by using the technique of on-line collinear fast atomic beam-laser spectroscopy [13] at the ISOLDE facility at CERN [14]*). The isotopes studied include 12 radioactive and 2 stable ones, and their hfs were investigated in two atomic transitions, $4f^7 6s^2\ {}^8S_{7/2} - 4f^7 6s6p,\ y\,{}^8P_{9/2,7/2}$ at 4594 Å and 4627 Å. The nuclear spins, magnetic dipole and electric quadrupole moments, and the changes in the mean square charge radii $\delta\langle r^2\rangle$, have been evaluated for the nuclear ground states and two isomeric states. The results for the neutron-deficient isotopes support a shell-model description with increasing collective effects on either side of the N = 82 shell closure in the range $140 \leq A \leq 151$ ($77 \leq N \leq 88$), whereas in the N = 89 and 90 nuclei, ^{152}Eu and ^{153}Eu, the interpretation has to include strong collective effects. In particular, ^{145}Eu has the features of a proton-hole state with respect to the doubly-magic configuration of ^{146}Gd [15].

---

*) The preliminary results of this investigation were already reported at the Sixth International Conference on Hyperfine Interactions and also at the 1983 International Conference on Nuclear Physics [3].

2. EXPERIMENTAL

2.1 Production of radioactive Eu isotopes

The experiments were performed at the ISOLDE facility [14] at CERN using mass-separated products of spallation reactions induced by 600 MeV protons in a Ta foil target (122 g/cm^2). During the operation the target is heated to 2200 °C in order to release the spallation products. The atoms are ionized on a hot (2400 °C) tungsten surface, which is in the form of an orifice of the target container. These ions are extracted to form a 60 keV beam and after mass separation they are directed to the set-up for collinear fast-beam laser spectroscopy. The investigated nuclides are listed in Table 1 and their production yield ranges between 10^6 and 10^9 ions/s.

2.2 The apparatus

The apparatus has been described in detail elsewhere [2]. Its essential features are:

i) the electrostatic deflection of the ion beam into the laser-beam axis;

ii) a charge-exchange cell at a variable potential to convert the ion beam into a fast atomic beam and to Doppler-tune the effective laser frequency;

iii) a detection chamber to observe fluorescence photons from laser-excited atoms;

iv) precision high-voltage scanning and measuring devices for controlling the Doppler shifts that correspond to the resonance frequencies to be determined.

2.3 High-resolution spectroscopy

The measurements have been carried out in the two Eu I transitions at 4627 Å and 4594 Å, connecting the $4f^7 6s^2\ {}^8S_{7/2}$ ground state with the $y^8P_{7/2}$ and $y^8P_{9/2}$ states, respectively, which belong to the parent terms $({}^8S_{7/2})({}^1P_1)$ of the configuration $4f^7 6s6p$. Previously, high-resolution studies in these two transitions were carried out for the two stable isotopes ^{151}Eu and ^{153}Eu by Zaal et al. [16]. The observed resonances for the odd-A isotopes $^{141-151}$Eu in the 4627 Å transition are presented in Fig. 1a, which shows the similarity of the hfs for all these $I = 5/2$ nuclides; the splitting is maximum for ^{145}Eu (N = 82) and decreases for both lower and higher masses.

The wide splitting is due to the excited state and the narrow one to the ground state (see Fig. 1b). Contributions to the observed 35 MHz line width are the natural width of 30 MHz, the residual Doppler width, and some power broadening. The integration times for the spectra shown in Fig. 1a range from 0.4 to 4.0 s per channel (500 channels) depending on the respective isotopic yields which have their maximum around ^{145}Eu.

Similar spectra have also been obtained in the 4594 Å transition. On the doubly-odd isotopes additional components from isomeric nuclear states are observed in ^{142}Eu and ^{150}Eu (see Fig. 2). For the evaluation of the IS, all spectra have been measured in an alternating mode with either ^{145}Eu or ^{151}Eu as the reference isotope.

3. RESULTS

The peak positions of all observed hfs components were determined with an accuracy corresponding to typically 1-10 MHz. After transformation from the voltage to the frequency scale, these positions were fitted with the hfs formula describing them in terms of the nuclear spin I, the ground- and excited-state dipole interaction constants A_g, A_e, and quadrupole interaction constants B_g, B_e, and the centre of gravity. Owing to the small and partially resolved ground-state splitting it was imperative to use fixed ratios A_e/A_g = 11.49(1) and 10.94(1), and B_e/B_g = -322(4) and 421(3) for the 4594 and 4627 Å lines, respectively; these values were taken from precision measurements on the stable isotopes by ABMR for the ground state [17] and by laser spectroscopy for the excited states [16]. The isotopic changes of these ratios (e.g. the hfs anomalies) are much smaller than the optical resolution of the ground-state splitting, which is treated as a correction for fitting essentially the excited-state hfs only. The nuclear spins and the A and B factors of the $y^8P_{7/2}$ and $y^8P_{9/2}$ excited states are listed in Table 2. The isotope shifts, i.e. the centres of gravity with respect to that of ^{145}Eu, are given in the first two columns of Table 3.

3.1 Nuclear moments

The nuclear magnetic moments μ were evaluated from the hyperfine constants using as reference the known value μ = 3.4717(6) n.m. of the magnetic moment of ^{151}Eu [12]. The dominating contribution to the magnetic dipole moments from the $2d_{5/2}$ proton in the range $140 \leq A \leq 151$ (cf. Sections 4.1 and 4.2) suggests a rather similar nuclear structure and thus a small hyperfine anomaly. This anomaly, defined as the relative difference of the A- and g_I-factor ratios between two isotopes, e.g.

$$^{151}\Delta^{153} = 1 - \frac{g_I^{153}}{g_I^{151}} \frac{A^{151}}{A^{153}} ,$$

has been investigated for the two stable isotopes by Zaal et al. [16] in both the $y^8P_{7/2}$ and $y^8P_{9/2}$ states. They are quite different, namely $^{151}\Delta^{153}(^8P_{7/2}) = -0.27(40)\%$ and $^{151}\Delta^{153}(^8P_{9/2}) = -1.33(18)\%$, and confirmed by our somewhat less accurate results. The rather large values are due to the change of the $^5/_2^+$ ground state from essentially a $\pi 2d_{5/2}$ shell-model state to a [413 $^5/_2$] Nilsson-model state, going along with a large drop in μ itself. The anomalies for the whole sequence of neutron-deficient isotopes should be considerably smaller. This is confirmed, for the isotopes $142 \leq A \leq 151$, by the observation that the ratios of the measured A factors of both states all agree with the one for ^{151}Eu, although the hyperfine anomaly in the one state should be about 5 times as large as that in the other [16]. Therefore, we have taken the magnetic moments calculated from the $yP_{7/2}$ splitting without introducing additional errors. This holds true also for the strongly-deformed ^{152}Eu, where the statistical error is larger than any expected hyperfine anomaly. The evaluated dipole moments are corrected for diamagnetism [12].

The quadrupole moments were evaluated taking as reference the value $Q_s = 2.412(21)$ b obtained for ^{153}Eu from the muonic X-rays [11]. The B factors are larger and are determined with better precision in the $y^8P_{7/2}$ level than in $y^8P_{9/2}$ so we have used the former for the evaluation of Q_s listed in Table 4. Generally the moments derived from the two states agree very well.

The final results are summarized in Table 4 together with previously known

moments. Comparison of different results shows that the magnetic moments of $^{145-148}$Eu, recently reported by van den Berg et al. [5], are apparently in error. Since there is no common scaling factor between our results and theirs, the errors have to be traced to the assumptions made for individual nuclei in their evaluation from the field dependence of nuclear orientation. The values reported for $^{145-149}$Eu by Kracikova et al. [6] are in qualitative agreement with our values. On the other hand, our values are in good agreement with the results for ^{147,149}Eu reported by Dörschel et al. [8b].

3.2 Isotope shift and evaluation of the nuclear parameter λ and the differences in mean square charge radii

The IS evaluated from the observed hfs in the 4594 Å and 4627 Å lines are listed in Table 3 with ^{145}Eu taken as reference. For the evaluation of the nuclear parameter λ from the IS, one first extracts the field shift (FS) $\delta\nu_{FS}$ by subtracting normal mass shift (NMS) and specific mass shift (SMS). In s^2-sp transition the SMS is usually neglected [18] and one takes only the NMS, which is given by $(\nu_i/1836.1)(A' - A)/(AA')$ where ν_i is the transition frequency.

The field shift $\delta\nu_{FS}$ between two isotopes A and A′ in a transition i can be written in the usual form [18]

$$\delta\nu_{i,FS}^{A,A'} = F_i \lambda^{A,A'} , \tag{1}$$

where F_i is the electronic factor and λ is the nuclear parameter which can be expressed as a power series of mean charge radii differences [19], in terms of C_n which are constants for a particular nuclear charge Z:

$$\lambda = \delta\langle r^2\rangle + \frac{C_2}{C_1}\,\delta\langle r^4\rangle + \frac{C_3}{C_1}\,\delta\langle r^6\rangle + \ldots \tag{2}$$

Equation (1) can be factorized as [18]:

$$\delta\nu_{i,FS}^{A,A'} = E_i f(Z) \lambda^{A,A'} , \tag{3}$$

where E_i is an electronic factor depending on the difference of total non-relativistic electron charge density at the nucleus between the initial and final electronic states

$$E_i = \pi a_0^3 \Delta|\psi(0)|_i^2 / Z \ . \qquad (4)$$

Here a_0 is the Bohr radius and $\Delta|\psi(0)|_i^2$ is the change in the electron-charge density at the nucleus for the particular transition. The factor f(Z) accounts for the relativistic correction to E_i and for the finite nuclear charge distribution. It is given as [18]

$$f(Z) = 5/2 \left(\frac{A+A'}{2}\right)^{1/3} C_{unif}^{A,A'} \Big/ \left[r_0^2 (A' - A)\right] , \qquad (5)$$

where $r_0 = 1.2$ fm and $C_{unif}^{A,A'}$ is the theoretical IS constant for a uniformly charged nuclear sphere of radius $R = r_0 A^{1/3}$. It can be evaluated by using the relation given by Babushkin [20] (corrected for the missing $(n/N)^3$ factor as suggested by Zimmermann [21]).

The IS in the 4627 Å and 4594 Å lines of Eu deviates considerably from the IS in other lines which are supposed to be transitions from a pure $4f^7 6s6p$ configuration to the ground state $4f^7 6s^2$. This deviation has been attributed to the influence of configuration mixing in the y^8P states of $4f^7 6s6p$ [16]. The maximum IS of a $4f^7 6s6p$-$4f^7 6s^2$ type transition is observed in the 5765 Å line, where the excited state $z^6P_{7/2}$ is supposed to have a pure configuration. Zaal et al. [16], Heinecke [22], and Alkhazov et al. [7] have measured the IS involving ^{151,153}Eu, ^{152}Eu, and $^{141-150}$Eu, respectively, in this line. We have related our IS values to those in the 5765 Å line by a King plot [18] (Fig. 3). Although not all the values reported by Alkhasov et al. [7] are consistent with ours within their relatively large errors, the combination of the data of Refs. [7], [16], and [22] gives rather accurate ratios of the field shifts in the 4594 Å and 4627 Å lines to the field shift in the 5765 Å line. From a least squares fit we obtain these ratios as 0.837(7) and 0.802(6), respectively. They were used to calibrate the F factor [Eq. (1)] in order to evaluate $\lambda^{A,A'}$ from the $\delta\nu_{FS}$ observed in the two transitions at 4594 Å and 4627 Å.

In the calculation of the electronic factor E_i [Eq, (4)] it is assumed that the contribution from p electrons can be neglected, so we have [18]

$$\Delta|\psi(0)|^2_{4f^7 6s^2 - 4f^7 6s6p} = -\gamma|\psi(0)|^2_{6s} \ .$$

The screening factor $\gamma = 0.73$ for Eu I has been evaluated relativistically by Coulthard [23]. Using the ionization potential of Eu II [24], we have evaluated the charge density $|\psi(0)|^2_{6s} = 8.23\ a_0^{-3}$ of the s electron in the configuration $4f^7 6s$ of singly ionized Eu II. With these values of γ and $|\psi(0)|^2$ in Eq. (4) we obtained $E_i = -0.2995$. The values of $f(Z)$ [see Eq. (5)] vary between 22.01 GHz/fm^2 for the isotope pair (140,141) to 21.87 GHz/fm^2 for (152,153). For a pure $4f^7 6s^2 - 4f^7 6s6p$ type transition of Eu the electronic factors F were evaluated with the parameters given above, e.g. $F^{151,153} = -6.55$ GHz/fm^2. Using the ratio of field shifts discussed in the preceding section, we obtained, for instance, $F^{151,153} = -5.48$ GHz/fm^2 and -5.25 GHz/fm^2 for the lines 4594 Å and 4627 Å, respectively. The $\lambda^{A,A'}$ values were evaluated from the observed $\delta\nu_{FS}^{A,A'}$ and F factors using relation (1), and are listed in Table 3.

The differences in the mean square charge radii $\delta\langle r^2\rangle^{A,A'}$ can be obtained from $\lambda^{A,A'}$ using the relation (2), which can also be expressed with the ratio $\delta\langle r^4\rangle/\delta\langle r^2\rangle$ and $\delta\langle r^6\rangle/\delta\langle r^2\rangle$ evaluated using a homogeneously charge sphere nucleus of radius R

$$\lambda^{A,A'} = \left(1 + \frac{C_2}{C_1}\frac{10}{7}\bar{R}^2 + \frac{C_3}{C_1}\frac{5}{3}\bar{R}^4\right)\delta\langle r^2\rangle \ , \qquad (6)$$

where $\bar{R} = 1.2\ \bar{A}^{1/3}$ fm and $\bar{A} = (A + A')/2$.

The relation (6) will not be valid if there are strong nuclear deformations present, since the contributions of higher order moments for a given $\delta\langle r^2\rangle$ will be different. Taking into account the deformation contribution of higher order moments, as discussed in detail by us elsewhere [25], $\lambda^{A,A'}$ can be expressed in terms of $\delta\langle r^2\rangle^{A,A'}$ as

$$\lambda^{A,A'} = \delta\langle r^2\rangle^{A,A'} + x\ \delta\langle r^2\rangle^{A,A'}_{sph} + y\ \frac{5}{4\pi}\overline{\langle r^2\rangle}_{sph}\ \delta\langle\beta_2^2\rangle^{A,A'} \ , \qquad (7)$$

where

$$x = \left[\frac{C_2}{C_1}\frac{10}{7}\bar{R}^2 + \frac{C_3}{C_1}\frac{5}{3}\bar{R}^4\right]$$

and

$$y = \left[\frac{C_2}{C_1}\,2\bar{R}^2 + \frac{C_3}{C_1}\,3\bar{R}^4\right] .$$

Here, we have assumed that $\delta\langle r^2\rangle$ can be decomposed [according to Eq. (9)] into a "spherical" part describing the change in nuclear volume and a "deformation" part at constant volume. The corresponding corrections have been applied after a preliminary calculation of $\delta\langle r^2\rangle$ according to Eqs. (3) and (6) and the decomposition using $\delta\langle r^2\rangle_{sph}$ from the droplet model [26]. The coefficients C_1, C_2, C_3 are taken from Seltzer [19]. The difference in the higher-moment correction for spherical and deformed nuclei is significant only for big changes in the deformation parameter β_2, i.e. between ^{151}Eu and ^{152,153}Eu [27]. The values of $\delta\langle r^2\rangle^{145,A}$ are presented in the last column of Table 4.

The comparison of our $\lambda^{151,153}$ and $\lambda^{151,152}$ values with earlier reported works [16,18,28,29] is shown in Table 5.

4. DISCUSSION

4.1 Nuclear spins

The nuclear spins of all the isotopes studied are listed in column 2 of Table 4. They are unambiguously determined from the hfs patterns as described in Section 3. Whereas in the cases of low spin ($I < J$) the number of components is simply determined by the spin value, the higher-spin cases require the exclusion of all but one spin value by the fitting procedure. For very high spins, the partially resolved spectra may be compatible with more than one spin assumption. In these cases (for ^{142m}Eu, in particular) the ambiguity is removed by verifying that the known A- and B-factor ratios of the $^8P_{7/2}$ and $^8P_{9/2}$ states are reproduced only for one of the possible spin values. All the spins previously determined by the ABMR technique [9,10] are confirmed. The spins of ^{140}Eu, ^{141}Eu, ^{142}Eu, ^{142m}Eu, ^{144}Eu, and ^{150}Eu have been directly determined for the first time in the present experiment. For ^{142}Eu and ^{142m}Eu the spin values of 1 and 7, respectively, were proposed by Kennedy et al. [30] on the basis of nuclear spectroscopy. We confirmed $I = 1$ for ^{142}Eu, but ^{142m}Eu has to be assigned $I = 8$. This value of I for ^{142m}Eu also explains the observed magnetic moment $\mu = 2.98$ nm, which should originate by coupling a $2d_{5/2}$ proton to a $1h_{11/2}$ neutron (our estimated values of μ are 2.59 and 1.66 nm for the spin values of 8 and 7, respectively). For ^{150}Eu

both I = 4 and 5 have been proposed on the basis of nuclear level structure studies [12]. Our analysis gives I = 5 (Fig. 2), which is preferred also by Soramel-Stanco et al. [31] in order to explain the observed isomers of ^{150}Eu and supported by their (p,n) data.

4.2 Nuclear moments

The nuclear magnetic dipole moments are given in column 3 of Table 4. The ground states of the odd-A transitional nuclei in the range $^{141-151}$Eu are associated with the $2d_{5/2}$ shell-model proton state. The magnetic moments of these isotopes are plotted against neutron numbers in Fig. 4, which nicely shows the maximum value of μ at N = 82 and decreasing values on either side of it. This maximum at ^{145}Eu reaches 83% of the Schmidt value. It shows that the reduction of single-particle moments by core polarization including collective modes is minimized at the shell closure. A similar behaviour is known for other $\pi d_{5/2}$ states in $^{17}_{9}F^{8}$, $^{141}_{59}Pr^{82}$, and $^{143}_{61}Pm^{82}$ [12]. Europium is now the longest chain for which the magnetic moments of isotopes with essentially identical shell-model proton states have been measured. Interacting-Boson-Model calculations [32] of the nuclear moments in the $^{147-151}$Eu range agree in magnitude and trend with the experimental data. The proton part of the doubly-odd isotopes $^{140-150}$Eu is shown also to be due to $2d_{5/2}$, coupled to a $2d_{3/2}$ neutron in ^{140,142,144}Eu, a $1h_{11/2}$ neutron in ^{142m}Eu, and a $2f_{7/2}$ neutron in $^{146-150}$Eu. It is shown in Table 6 that the magnetic moments of these doubly-odd isotopes are qualitatively reproduced by the additivity theorem

$$\mu_I = \frac{I}{2}\left[g_p + g_n + (g_p - g_n)\,\frac{j_p(j_p+1) - j_n(j_n+1)}{I(I+1)}\right], \qquad (8)$$

using empirical proton and neutron g factors from the neighbouring nuclei (j_p and j_n are the angular momenta of the proton and neutron shell-model states, respectively).

The magnetic moment of the strongly deformed nucleus ^{153}Eu is well accounted for by the Nilsson proton orbital [413 5/2] with deformation of $\beta_2 \approx 0.30$ [33]. Similarly the moment of the spin I = 3 state in the doubly-odd isotope ^{152}Eu is

well described by the configuration $\{\pi[413\ 5/2]\nu[505\ 11/2]\}$, for which we obtain a Nilsson-model prediction of -1.82.

The Q_s values of the odd-even isotopes with a $5/2^+$ proton state are plotted against neutron number N in Fig. 4, where we get a minimum at the shell closure (N = 82) and increasing values on either side of it with a big jump at the shape transition between N = 88 and N = 90.

At the shell-closure minimum, a roughly-estimated single-particle value of $Q_{sp} = \{(2j-1)/(2j+1)\}\langle r^2\rangle = 0.13$ b accounts for 50% of the observed value $Q_s(^{145}Eu) = 0.28$ b. The small residual core polarization is similar to analogous cases of single-particle or hole states in a doubly-magic core (e.g. ^{209}Bi, where $Q_{sp} = 0.21$ b and $Q_s = 0.4$ b).

Prior to the muonic X-ray studies [11] the Q_s values of ^{151}Eu and ^{153}Eu were known from the analysis of optical hfs. The uncorrected values of Q_s' were reported by Bordarier et al. [34] and Guthörlein et al. [35]. Bordarier et al. analysed the hfs of $4f^76s^2$-$4f^76s6p$ transitions of Eu I. From six B factors for ^{151}Eu and three B factors for ^{153}Eu they reported $Q_s'(^{151}Eu) = 1.16(8)$ b and $Q_s'(^{153}Eu) = 2.92(20)$ b. Guthörlein et al. analysed the hfs of $4f^76p$-$4f^76s$ transitions of Eu II. From the data obtained for three levels of $4f^76p$ they reported $Q_s'(^{151}Eu) = 1.12(7)$ b and $Q_s'(^{153}Eu) = 2.85(18)$ b. These $Q_s'(6p)$ values have to be corrected by the Sternheimer quadrupole shielding or antishielding factors R(6p) according to the equation $Q_s = Q_s'(6p)/[1-R(6p)]$. With the Sternheimer correction of R(6p) = -0.18(5) [36], we obtained a corrected mean value of $Q_s(^{151}Eu) = 0.97(10)$ b and $Q_s(^{153}Eu) = 2.44(27)$ b, which can be compared with the muonic values of $Q_s(^{151}Eu) = 0.903(10)$ b and $Q_s(^{153}Eu) = 2.412(21)$ b [11]*).

4.3 Mean square charge radii

The $\delta\langle r^2\rangle$ values of the isotopes in the range $^{140-153}Eu$ are plotted in Fig. 5 with ^{145}Eu (N = 82) as reference. The values of $\delta\langle r^2\rangle_{sph}$ from the spherical-droplet model [26] are also plotted in Fig. 5. As can be seen from the figure, except

*) $Q_s'(5d)$ have been reported by Brand et al. [28] for Eu I and by Arnesen et al. [37] for Eu II; owing to the uncertainty about R(5d), as discussed in Ref. [28], these values are not included in our discussion.

for ^{144}Eu, the $\delta\langle r^2\rangle$ observed deviates from the spherical droplet line, showing the development of deformation on both sides of neutron shell closure at N = 82. The lines of constant deformation in Fig. 5 have been calculated by using the standard formula including the quadrupole deformation β_2 with conserved nuclear volume

$$\delta\langle r^2\rangle^{A,A'} = \delta\langle r^2\rangle^{A,A'}_{sph} + \frac{5}{4\pi}\overline{\langle r^2\rangle}_{sph}\,\delta\langle\beta_2^2\rangle^{A,A'} \qquad (9)$$

in the modified form where the contribution to $\langle r^2\rangle$ from redistribution and its shape dependence is taken into account according to the latest version of the droplet model [26]. On the lighter mass side the collective effects are strong enough to change the sign of $\delta\langle r^2\rangle$ of ^{140}Eu (N = 77) and ^{141}Eu (N = 78) relative to ^{145}Eu. On the higher mass side the deformation develops slowly as the neutrons are added to the closed shell; and then there is a steep increase to strong static deformation between N = 88 and 89*), whereas, above N = 89, and in particular between ^{152}Eu (N = 89) and ^{153}Eu (N = 90), the deformation remains almost constant, as shown earlier also by Heinecke [22]. The isomer shift between ^{142g}Eu and ^{142m}Eu is 0.057 fm^2, showing that the high-spin isomer is more collective than the ground state, whereas the isomer shift between ^{150g}Eu and ^{150m}Eu (N = 87) is small.

According to Eq. (9) the deformation parameter β_2 of statically deformed nuclei can be evaluated from $\delta\langle r^2\rangle^{A,A'}$, if the $\langle\beta_2^2\rangle$ is known for one isotope. Assuming $\langle\beta_2^2\rangle = 0$ for ^{145}Eu we have evaluated the deformation parameter β_2 of ^{152}Eu and ^{153}Eu. We obtain $\beta_2 = 0.32$ for both ^{152}Eu and ^{153}Eu. These can be compared with $\beta_2 = 0.31$ evaluated from $Q_0 = 6.69$ b of ^{153}Eu [27] obtained from B(E2) values. With $Q_0 = 6.75$ b for ^{153}Eu, obtained using the strong coupling projection formula $Q_0 = [(I+1)(2I+3)/I(2I-1)]Q_s$ and $Q_s = 2.412(21)$ b reported by Tanaka et al. [11], we get $\beta_2 = 0.32$. The consistency of all these values is excellent and supports the analyses and the assumptions involved, namely the

*) Because of historical reasons (the early IS studies were only between even-even isotopes) it is usually stated in the literature that the big jump in deformation is between N = 88 and 90.

static deformation parameter value of ^{153}Eu, our evaluation of $\lambda^{A,A'}$ and $\delta\langle r^2\rangle$, and the new calibration values for Q_s obtained from muonic X-ray studies.

The value of $\delta\langle r^2\rangle^{151,153} = 0.602(33)$ fm^2, obtained by applying the higher-order charge moment correction to our $\lambda^{151,153}$ value, is in excellent agreement with the muonic X-ray value of $\delta\langle r^2\rangle^{151,153} = 0.606(18)$ fm^2 [38].

5. CONCLUSION

The present investigation of hyperfine structures and isotope shifts in a long isotopic chain of neutron-deficient isotopes of Eu has considerably extended our knowledge of their nuclear ground and isomeric state properties, which are summarized below.

i) The nuclear spins of ^{140}Eu, ^{141}Eu, ^{142}Eu, ^{144}Eu, ^{150}Eu, and the isomer ^{142m}Eu have been directly measured.

ii) The magnetic dipole moments of isotopes in the $^{140-150}$Eu range have been determined from the atomic hfs. They resolve the existing discrepancy in the reported values for a few isotopes in this region. The values of quadrupole moments in $^{140-150}$Eu are the first ones to be reported. The nuclear moments of ^{145}Eu are well understood in terms of a $(\pi 2d_{5/2})^{-1}$ hole state to a doubly-magic ^{146}Gd core. On either side of the N = 82 shell closure, the moments indicate increasing collective effects and the well-known onset of strong static ground-state deformation between N = 88 and 89.

iii) The variation of $\delta\langle r^2\rangle$ with neutron number N in Eu, below and above the shell closure (N = 82), shows a different characteristic compared to other elements in which long isotopic chains have been investigated, e.g. Ba, Cs, Xe [2] and other rare-earths [1]. For $N \leq 80$ the mean square charge radii start to increase again. Above N = 82, the complete measurement of the $\delta\langle r^2\rangle$ sequence between the strongly deformed ^{153}Eu and the spherical ^{145}Eu confirms that the N = 88-90 shape transition is most pronounced in Eu.

Acknowledgement

We are grateful to Professor E.-W. Otten for helpful discussions and suggestions during the preparation of the paper. We would like to thank Professor R.M. Steffen for making available to us material not yet published.

This work was supported by the Bundesministerium für Forschung und Technologie and the Deutsche Forschungsgemeinschaft.

REFERENCES

[1] R. Neugart, *in* Lasers in Nuclear Physics (C.E. Bemis, jr., and H.K. Carter), Nuclear Science Research Conference Series, Vol. 3 (Harwood, Chur-London-New York, 1982), p. 231.

[2] A.C. Mueller, F. Buchinger, W. Klempt, E.W. Otten, R. Neugart, C. Ekström and J. Heinemeier, Nucl. Phys. A403 (1983) 234.

[3] a) R. Neugart, K. Wendt, S.A. Ahmad, W. Klempt and C. Ekström, Hyperfine Interactions 15/16 (1983) 181.

b) S.A. Ahmad, F. Buchinger, C. Ekström, W. Klempt, A.C. Mueller, R. Neugart, E.W. Otten and K. Wendt, Nuclear spins, moments and mean square charge radii of unstable nuclides in the region N ≈ 82, Proc. Int. Conf. on Nuclear Physics, Florence, 1983 (Tripografia Compositori, Bologna, 1983), vol. 1, p. B262.

[4] P. Brix, Z. Phys. 132 (1952) 579.

[5] F.G. van den Berg, W. van Rijswijk and W.J. Huiskamp, Phys. Lett. 120B (1983) 67.

[6] T.I. Kracikova, S. Davaa, M. Finger and V.A. Deryuga, Hyperfine Interactions 15/16 (1983) 73.

[7] a) G.D. Alkhazov, A.E. Barzakh, E.I. Berlovich, V.P. Denisov, A.G. Dernyatin, V.S. Ivanov, A.N. Zherikhin, O.N. Kompanets, V.S. Letokhov, V.I. Mishin and V.N. Fedoseev, JETP Lett. 37 (1983) 274.

b) A.N. Zherikhin, O.N. Kompanets, V.S. Letokhov, V.I. Mishin, V.N. Fedoseev, G.D. Alkhazov, A.E. Barzakh, E.E. Berlovich, V.P. Denisov. A.G. Dernyatin and V.S. Ivanov, Zh. Eksp. Teor. Fiz. 86, (1984) 1249.

[8] a) K. Dörschel, W. Heddrich, H. Hühnermann, E.W. Peau, W. Wagner, G.D. Alkhazov, E.Ye. Berlovich, V.P. Denisov, V.N. Panteleev and A.G. Polyakov, Z. Phys. A 312 (1983) 269.

b) K. Dörschel, W. Heddrich, H. Hühnermann, E.W. Peau, W. Wagner, G.D. Alkhazov, E.Ye. Berlovich, V.P. Denisov, V.N. Panteleev and A.G. Polyakov, Z. Phys. A 317 (1984) 233.

[9] C. Ekström, S. Ingelman, M. Olsmats and B. Wannberg, Phys. Scr. 6 (1972) 181.

[10] C. Ekström and L. Robertsson, Z. Phys. A 302 (1981) 181 and A 316 (1984) 239.

[11] Y. Tanaka, R.M. Steffen, E.B. Shera, W. Reuter, M.V. Hoehn and J.D. Zumbro, Phys. Rev. Lett. 51 (1983) 1633.

[12] C.M. Lederer and V.S. Shirley, Table of Isotopes (Wiley, New York, 1978), 7th edn.

[13] K.R. Anton, S.L. Kaufman, W. Klempt, G. Moruzzi, R. Neugart, E.W. Otten and B. Schinzler, Phys. Rev. Lett. 40 (1978) 642.

[14] H.L. Ravn, Phys. Rep. 54 (1979) 201.

[15] M. Ogawa, R. Broda, K. Zell, P.J. Daly and P. Kleinheinz, Phys. Rev. Lett. 41 (1978) 289.

[16] G.J. Zaal, W. Hogervorst, E.R. Eliel, K.A.H. van Leeuwen and J. Blok, Z. Phys. A 290 (1979) 339.

[17] P.G.H. Sandars and G.K. Woodgate, Proc. R. Soc. London Ser. A, 257 (1960) 269.

[18] K. Heilig and A. Steudel, At. Data Nucl. Data Tables 14 (1974) 613.

[19] E.C. Seltzer, Phys. Rev. 188 (1969) 1916.

[20] F.A. Babushkin, Sov. Phys.-JETP 17 (1963) 1118.

[21] D. Zimmermann, Z. Phys. A 315, (1984) 123.

[22] P. Heinecke, Z. Phys. 245 (1971) 411.

[23] M.A. Coulthard, J. Phys. B. 6 (1973) 23.

[24] W.C. Martin, Romuald Zalubas and Lucy Hagan, Atomic Energy Levels - The rare-earth elements, NSRDS-NBS 60 (National Bureau of Standards, Washington, 1978).

[25] S.A. Ahmad, W. Klempt, R. Neugart, E.W. Otten, K. Wendt and C. Ekström, Isotope shifts, changes in the mean square charge radius and deformations of radium isotopes in the mass range $208 \leq A \leq 232$ (to be submitted to Nucl. Phys. A).

[26] W.D. Myers and K.H. Schmidt, Nucl. Phys. A 410 (1983) 61.

[27] K.E.G. Löbner, M. Vetter and V. Hönig, Nucl. Data Tables A7 (1970) 495.

[28] H. Brand, V. Pfeufer and A. Steudel, Z. Phys. A 302 (1981) 291.

[29] F. Boehm and P.L. Lee, At. Data Nucl. Data Tables 14 (1974) 605.

[30] G.G. Kennedy, S.C. Gujrathi and S.K. Mark, Phys. Rev. C 12 (1975) 553.

[31] F. Soramel-Stanco, R. Julin, J. Styczen, P.T. Prokofjev, A. Ercan and P. Kleinheinz, Z. Phys. A 314 (1983) 127.

[32] O. Scholten and N. Blasi, Nucl. Phys. A 380 (1982) 509.

[33] C. Ekström and I.-L. Lamm, Phys. Scr. 7 (1973) 31.

[34] Y. Bordarier, B.R. Judd and M. Klapisch, Proc. R. Soc. London Ser. A 289 (1965) 81.

[35] G. Guthörlein, G. Himmel and S. Steudel, J. Phys. (Paris) 30, Colloque C1 (1969) 66.

[36] R.M. Sternheimer (private communication).

[37] A. Arnesen, A. Bengtson, R. Hallin, C. Nordling, Ö. Staff and L. Ward, Phys. Scr. 24 (1981) 747.

[38] Y. Tanaka, R.M. Steffen, E.B. Shera, W. Reuter, M.V. Hoehn and J.D. Zumbro, Phys. Rev. C 29 (1984) 1897.

Table 1

Half-lives of the radioactive isotopes whose hfs has been investigated in the present study (from Karlsruher Nuklidkarte 1981)

A	Half-life	A	Half-life	A	Half-life
140	1.3 s	144	10 s	149	93 d
141	40 s	145	5.9 d	150	36 y
142	2.4 s	146	4.5 d	150^{m}	12.6 h
142^{m}	73 s	147	24.6 d	152	13 y
143	2.6 min	148	55.6 d		

Table 2

Nuclear spins and hfs constants evaluated from the measurements in the 4627 Å ($4f^7 6s^2\ {}^8S_{7/2}$-$4f^7 6s6p, y^8P_{7/2}$) and 4594 Å ($4f^7 6s^2\ {}^8S_{7/2}$-$4f^7 6s6p, y^8P_{9/2}$) lines of Eu I

A	I	Hyperfine constants			
		$4f^7 6s6p, y^8P_{7/2}$		$4f^7 6s6p, y^8P_{9/2}$	
		A (MHz)	B (MHz)	A (MHz)	B (MHz)
140	1	-215.3(2.0)	-98(12)		
141	5/2	-220.4(4)	-266(11)		
142	1	-242.2(2.9)	-37(17)	-253.6(3.8)	27(18)
142^m	8	-58.7(2)	-441(17)	-61.4(2)	319(19)
143	5/2	-231.7(4)	-160(8)	-242.3(4)	125(13)
144	1	-298.6(2.0)	-30(7)	-312.9(1.1)	21(8)
145	5/2	-251.9(3)	-90(6)	-263.5(4)	70(12)
146	4	-56.2(4)	56(17)	-58.6(2)	-67(10)
147	5/2	-234.9(4)	-172(8)	-245.9(4)	122(13)
148	5	-73.8(3)	-110(18)	-77.0(2)	77(12)
149	5/2	-224.9(3)	-234(6)	-235.7(4)	181(13)
150	5	-85.4(3)	-353(13)	-89.1(2)	254(12)
150^m	0	-	-	-	-
151	5/2	-218.6(4) -219.1(2) a)	-296(7) -295(3) a)	-229.0(5) -228.9(2) a)	228(11) 226(4) a)
152	3	102.8(2.6)	-793(67)		
153	5/2	-97.0(8) -97.0(4) a)	-760(15) -753(7) a)	-102.9(5) -102.4(2) a)	573(11) 575(8) a)

a) Ref. [16].

Table 3

Isotope shifts and nuclear parameters λ evaluated from the measurements in the 4627 Å and 4594 Å lines of Eu I. The common reference isotope is ^{145}Eu.

A	$\delta\nu^{145,A}$ (MHz)		$\lambda^{145,A}$ (fm^2)
	4627 Å	4594 Å	
140	-235(11)		0.028(12)
141	-231(6)		0.031(9)
142	230(14)	229(19)	-0.053(10)
142^m	-56(7)	-64(9)	0.001(6)
143	101(5)	92(7)	-0.026(5)
144	238(8)	239(8)	-0.048(6)
145	0	0	0
146	-607(10)	-620(8)	0.118(9)
147	-1325(5)	-1384(6)	0.258(17)
148	-1843(9)	-1902(8)	0.359(24)
149	-2602(5)	-2708(7)	0.507(33)
150	-3056(7)	-3177(7)	0.596(39)
150^m	-3100(10)	-3225(10)	0.605(40)
151	-4170(6)	-4343(9)	0.811(51)
152	-6879(18)		1.329(81)
153	-7146(9)	-7446(11)	1.383(83)

a) The estimated error in λ takes into account the error of the IS measurement, an assumed uncertainty of 5% in the evaluation of the F-factor, and (0 ± 0.5)NMS for the SMS. Except for $^{140-144}$Eu, where the IS is small, the major contribution is from the uncertainty in the F-factor.

Table 4

Nuclear spins, magnetic dipole and electric quadrupole moments, and differences in mean square charge radii of the isotopes in the range $^{140-153}$Eu

A	I	μ (n.m.)	Q_s (b)	$\delta\langle r^2\rangle^{145,A}$ (fm^2)
140	1	1.365(13)	0.31(4)	0.033(12)
141	5/2	3.494(8)	0.85(4)	0.035(9)
142	1	1.536(19)	0.12(5)	-0.054(10)
142^m	8	2.978(11)	1.41(6)	0.003(6)
143	5/2 a)	3.673(8)	0.51(3)	-0.026(5)
144	1	1.893(13)	0.10(3)	-0.050(6)
145	5/2 b)	3.993(7) ±1.1(3) d) ±3.2(5) e)	0.29(2)	0
146	4 b)	1.425(11) ±0.70(7) d) ±1.7(3) e)	-0.18(6)	0.124(9)
147	5/2 b)	3.724(8) ±1.0(1) d) ±3.1(4) e) 3.72 f)	0.55(3) 0.54 f)	0.271(17)
148	5 b)	2.340(10) ±1.33(6) d) ±2.1(3) e)	0.35(6)	0.376(24)
149	5/2 b)	3.565(6) ±2.5(5) e) 3.56 f)	0.75(2) 0.74 f)	0.532(33)
150	5	2.708(11)	1.13(5)	0.625(39)
150^m	0 b)	-	-	0.634(40)
151	5/2 c)	3.4717(6) c)	0.95(3) 0.903(10) g) 0.95 f)	0.851(51)
152	3 c)	-1.96(6) -1.9414(13) c)	2.54(22) 2.87 f)	1.396(81)
153	5/2 c)	1.538(13) 1.5330(8) c)	2.412(21) g) 2.43 f)	1.453(83)

a) Ref. [10], b) Ref. [9], c) Ref. [12]. d) Ref. [5], e) Ref. [6], f) Ref. [8b], g) Ref. [11].

Footnote to Table 4

The underlined figures represent the common reference values used for the evaluation of μ and Q_s. Tabulated quadrupole moments from optical hfs for ^{151,152,153}Eu (see, for example, Ref. [12]) do not include the Sternheimer correction. They are omitted in the present compilation.

h) See footnote of Table 3 for the error evaluation. No additional error is assumed for the Selzer correction.

Table 5

Comparison of $\lambda^{151,153}$ and $\lambda^{151,152}$ with earlier reported values

Isotope pair	λ [a] (fm^2)	$\delta\langle r^2\rangle$ (fm^2)	Transition studied		Ref.
(151,153)	0.572(33)	0.602(33)	$4f^76s^2$-$4f^76s6p$	Eu I	Present work
	0.571(46) [b]		$4f^76s^2$-$4f^76s6p$ $4f^75d6s$-$4f^75d6p$	Eu I	[18]
			$4f^76s$-$4f^75d$	Eu II	
	0.587(25) [b]		$4f^75d6s$-$4f^75d6p$		[28]
	0.550(35) [b] 0.580(35) [b]		$4f^76s$-$4f^75d$	Eu II	[28]
	0.591(7) [b]		$4f^76s^2$-$4f^76s6p$	Eu I	[16]
	0.581(31)		K_α X-ray		[29]
(151,152)	0.518(30)	0.545(30)	$4f^76s^2$-$4f^76s6p$	Eu I	Present work
	0.529(42)		$4f^76s^2$-$4f^76s6p$	Eu I	[18]

a) The quoted errors taken from the references are based on somewhat arbitrary assumptions (see Table 2). Therefore, they should not be compared without reconsideration.

b) Though given in the literature [16,18,28,29] as $\delta\langle r^2\rangle^{A,A'}$, they are actually $\lambda^{A,A'}$.

Table 6

Comparison of calculated semi-empirical magnetic moments μ_{se} (using additivity theorem) and experimental ones μ_{exp} for the doubly-odd Eu isotopes

A	I	Parameters used to calculate μ_{se} [a]		μ_{se}	μ_{exp}
		g_p	g_n		
140	1	1.40 ($2d_{5/2}$ ^{141}Eu)	0.46 ($2d_{3/2}$ ^{131}Xe)	2.10	1.37
142	1	1.43 ($2d_{5/2}$ ^{141,143}Eu)	0.56 ($2d_{3/2}$ ^{135}Ba)	2.09	1.54
144	1	1.53 ($2d_{5/2}$ ^{143,145}Eu)	0.62 ($2d_{3/2}$ ^{137}Ba)	2.21	1.89
142^m	8	1.43 ($2d_{5/2}$ ^{141,143}Eu)	-0.18 ($1h_{11/2}$ ^{137m}Ba) [b]	2.59	2.98
146	4	1.54 ($2d_{5/2}$ ^{145,147}Eu)	-0.26 ($2f_{7/2}$ ^{145}Sm)	1.30	1.43
148	5	1.46 ($2d_{5/2}$ ^{147,149}Eu)	-0.23 ($2f_{7/2}$ ^{147}Sm)	2.08	2.34
150	5	1.41 ($2d_{5/2}$ ^{149,151}Eu)	-0.19 ($2f_{7/2}$ ^{149}Sm)	2.11	2.71

a) The values of g_p are derived from the present measurement, whereas g_n are derived from μ values listed in Ref. [12].

b) Ref. [2].

Figure captions

Fig. 1 : a) Observed resonance patterns for odd-A isotopes $^{141-151}$Eu in the 4627 Å line, showing the similarity of the hfs due to essentially the $(2d_{5/2})^{-1}$ proton hole. The IS is disregarded.

b) Hfs splitting of the ground and the excited state (not to scale).

Fig. 2 : Hfs of ^{150}Eu in the 4594 Å line. The observed components can be explained only with I = 5. The values of F for the ground state (F_g) and the excited state (F_e) are given at the top. The additional single component is attributed to the I = 0 isomer ^{150m}Eu.

Fig. 3 : King plot of the IS in the 5765 Å [7, 16, 22], 6049 Å [8] and 4594 Å lines versus those in the 4627 Å line. The common reference isotope is ^{151}Eu.

Fig. 4 : Plot of magnetic (μ) and quadrupole (Q_s) moments of the $5/2^+$ ground states of Eu as a function of neutron number N. The quantities μ and Q_s, respectively, show a maximum and minimum at shell closure (N = 82). The values of the strongly-deformed ^{155}Eu are taken from ref. [8b].

Fig. 5 : Change of mean square charge radii $\delta\langle r^2\rangle$ in the isotopic chain $^{140-153}$Eu as a function of neutron number N, with ^{145}Eu (N = 82) taken as reference point. The change in deformation $\delta\langle\beta^2\rangle^{\frac{1}{2}}$, with respect to N = 82, is indicated by the parallel lines, the slope of which is given by the droplet model.

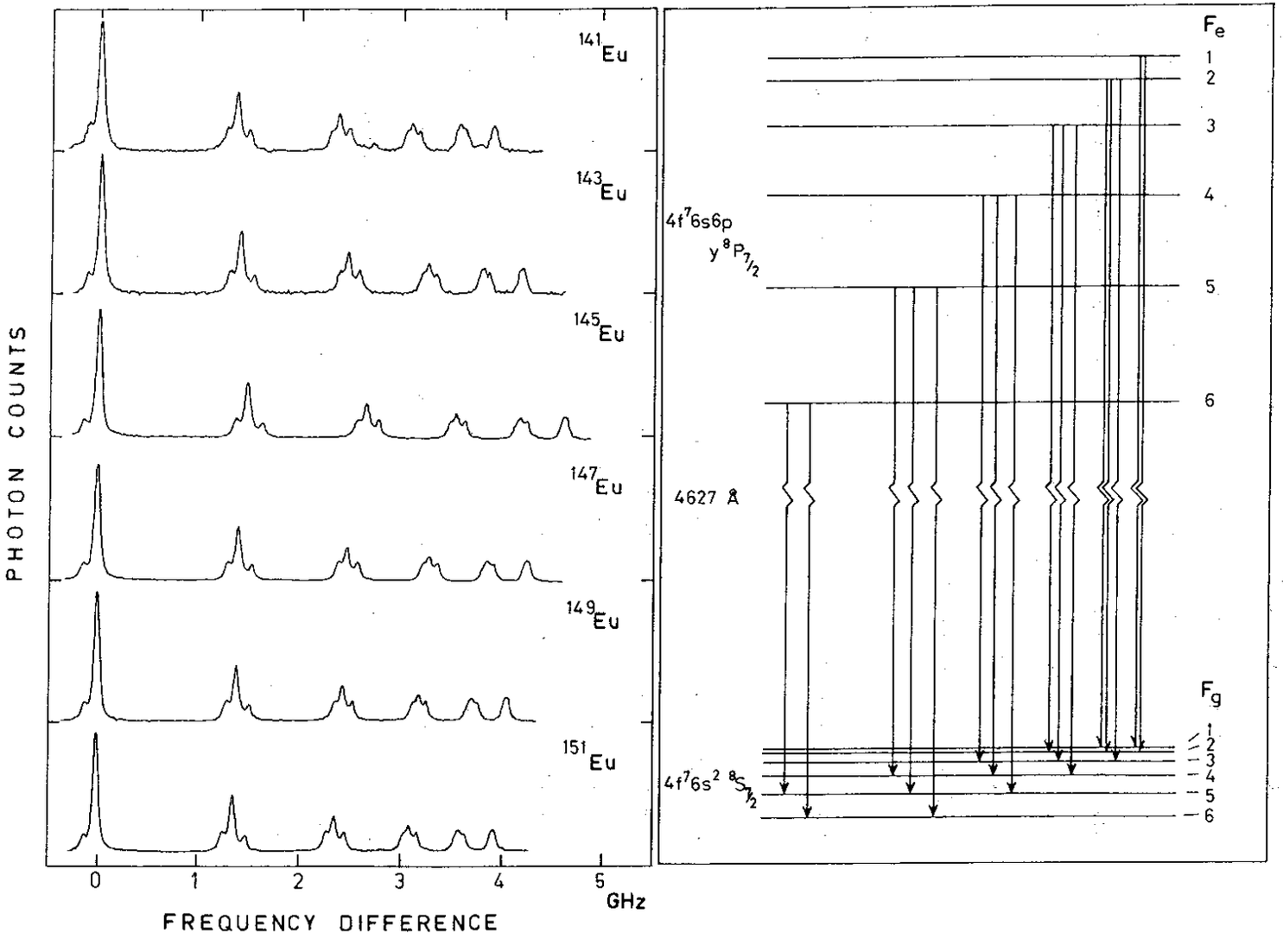
PHOTON COUNTS
141Eu
143Eu
145Eu
147Eu
149Eu
151Eu
0
1
2
3
4
5
GHz
FREQUENCY DIFFERENCE
Fe
1
2
3
4
5
6
4f76s6p
y 8P7/2
4627 Å
Fg
1
2
3
4
5
6
4f76s2 8S7/2

Fig. 1

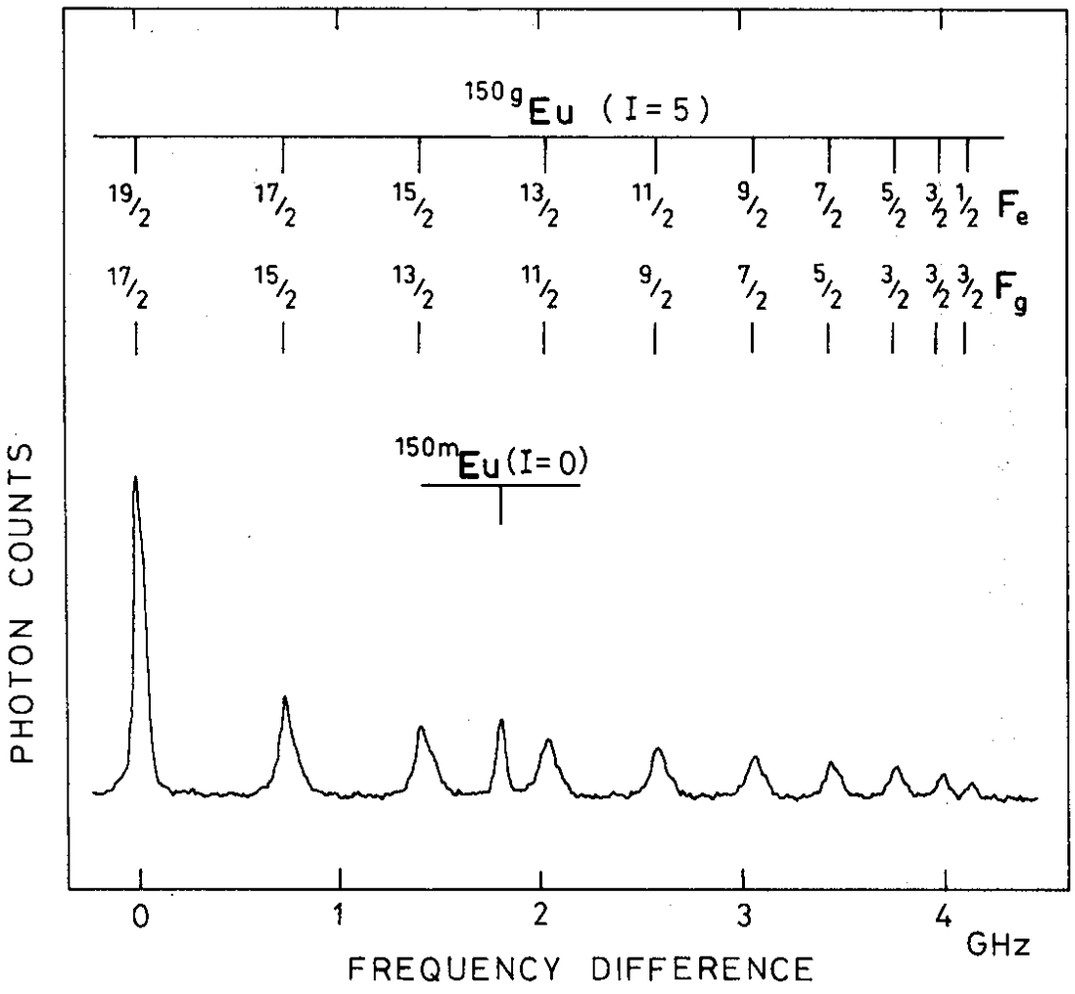
150g Eu (I=5)
19/2 17/2 15/2 13/2 11/2 9/2 7/2 5/2 3/2 1/2 Fe
17/2 15/2 13/2 11/2 9/2 7/2 5/2 3/2 3/2 3/2 Fg
150m Eu (I=0)
PHOTON COUNTS
0 1 2 3 4 GHz
FREQUENCY DIFFERENCE

Fig. 2

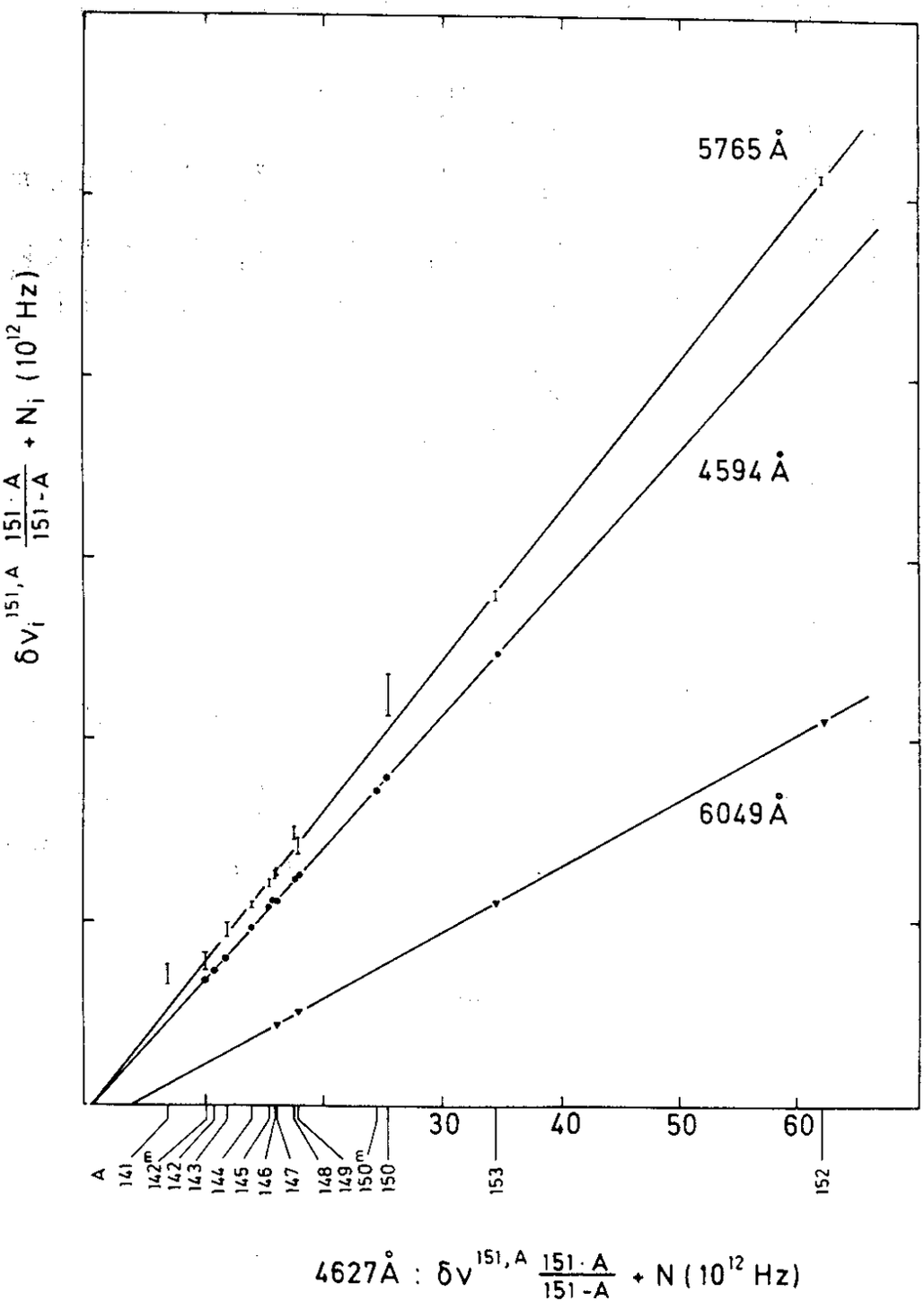
5765 Å
4594 Å
6049 Å
$\delta\nu_i^{151,A}\ \frac{151\cdot A}{151-A} + N_i\ (10^{12}\,Hz)$
A
141
142m
142
143
144
145
146
147
148
149
150m
150
153
152
30
40
50
60
$4627Å : \delta\nu^{151,A}\ \frac{151\cdot A}{151-A} + N\ (10^{12}\,Hz)$

Fig. 3

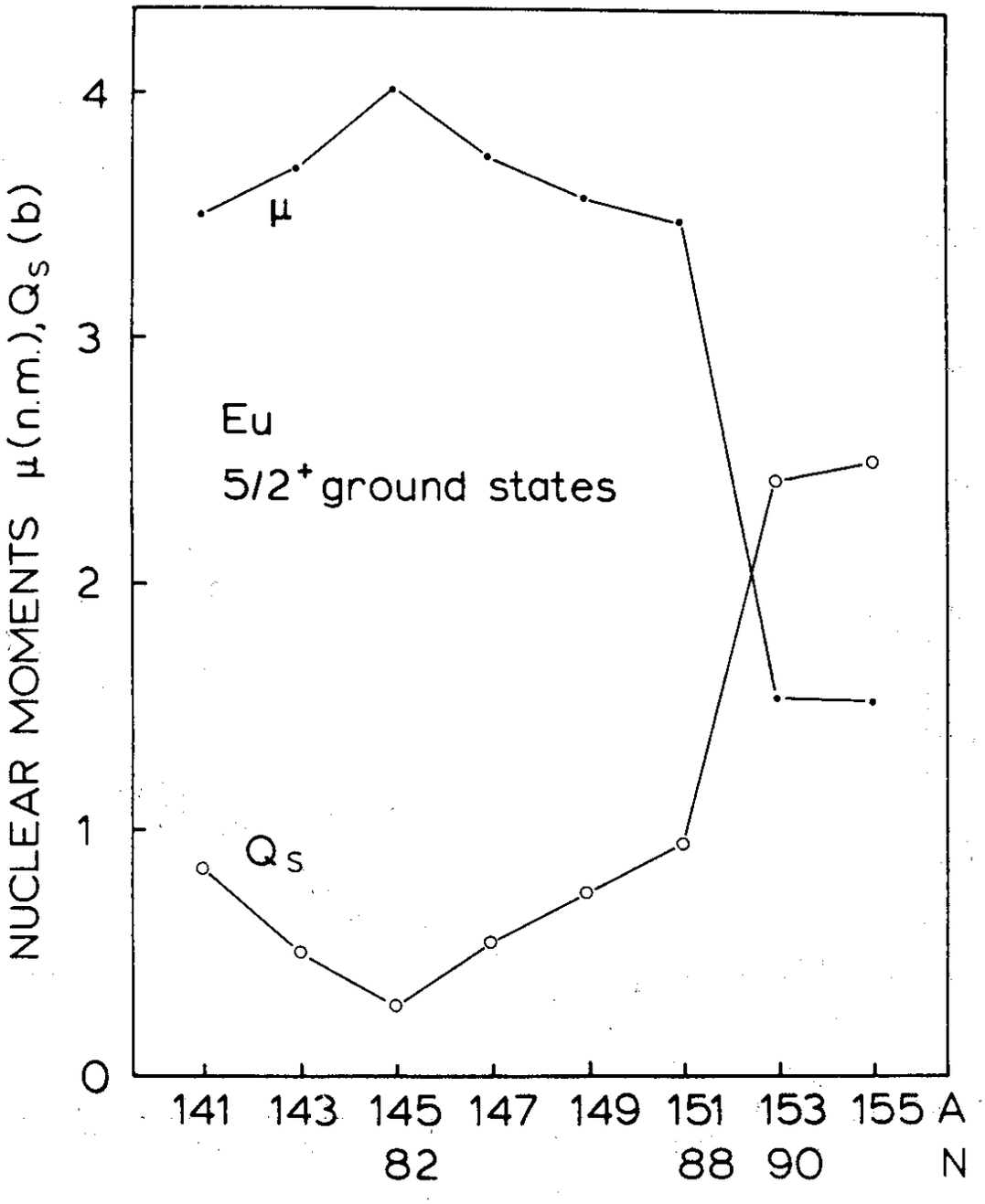
NUCLEAR MOMENTS μ(n.m.), Qs (b)
4
3
2
1
0
μ
Eu
5/2+ ground states
Qs
141
143
145
147
149
151
153
155
A
82
88
90
N

Fig. 4

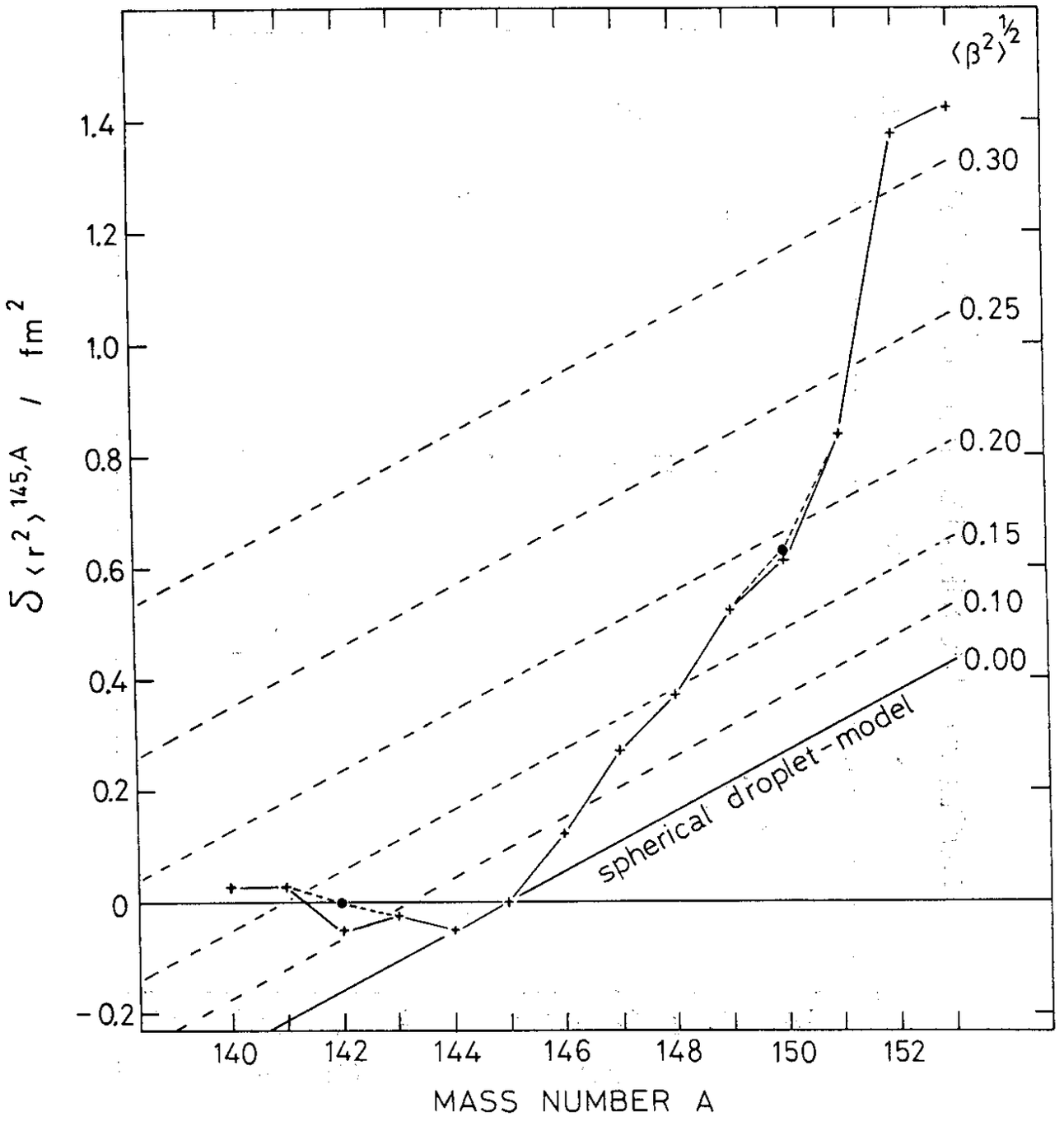
$\delta\langle r^2\rangle^{145,A}$ / fm^2
$\langle\beta^2\rangle^{1/2}$
1.4
1.2
1.0
0.8
0.6
0.4
0.2
0
-0.2
0.30
0.25
0.20
0.15
0.10
0.00
spherical droplet-model
140
142
144
146
148
150
152
MASS NUMBER A

Fig. 5